



High Lift Design and Aerodynamic Assessment for an Over-the-Wing Pylon-Mounted Engine Configuration with STOL Capabilities

L. Savoni¹, R. Rudnik,² A. Ronzheimer¹
DLR, Braunschweig, Germany, 38108

and

C. Heykena³
Technical University, Braunschweig, Germany, 38108

A CFD-based assessment of the low speed high lift performance of an over-the-wing mounted engine installations for a short range airliner with STOL capabilities is presented in this paper. The configuration is representative for a 100 passenger aircraft and characterized by pylon mounted over-the-wing installed UHBR-engines. The high lift system features active segmented and highly deflected Coanda flaps and a specifically designed droop nose at the leading edge of the wing. The study is part of the Collaborative Research Center 880 that develops technologies and configurations with quite STOL capabilities. The layout of the high lift system is described, together with the numerical approach and results for the considered test case. The objective of the present study is to investigate a short chord active plain flap in landing configuration and assess the maximum lift capabilities against target values from preliminary design studies of the CRC 880. It is a first step towards a more comprehensive assessment of variants of the high lift system. With the typical lift generation for a circulation control supported high lift system, the analysis of the stall behavior reveals a favorable smooth lift breakdown starting at the inner wing. Yet, the maximum lift properties fall short of the target value, so that an enlarged chord flap will be considered as a next step to comply with the maximum lift requirements.

Nomenclature

A	= reference area	<i>Greek symbols</i>
b	= wing span	α = angle of attack
BPR	= Bypass ratio	α_0 = angle of attack for zero lift generation
C_p	= pressure coefficient	α_{\max} = angle of attack for $C_{L,\max}$
C_L	= total lift coefficient	δ_{dn} = droop nose deflection angle
c	= chord length	δ_f = flap deflection angle
h	= height	δ_{ai} = aileron deflection angle
lct.	= lift count (=0.01)	Λ = aspect ratio
M	= Mach number	λ = taper ratio
Re	= Reynolds number based on c_{ref}	η = normalized span coordinate
s	= half span	<i>subscripts</i>
UHBR	= Ultra High Bypass Engine	∞ = free stream value

¹ Research Scientist, DLR, Institute of Aerodynamics and Flow Technology, Lilienthalplatz 7, 38108, Braunschweig, Germany..

² Head Transport Aircraft Department, DLR, Institute of Aerodynamics and Flow Technology, Lilienthalplatz 7, 38108, Braunschweig, Germany.

³ Research Scientist, TU-Braunschweig, Institute of Jet Propulsion and Turbomachinery (IFAS), Hermann-Blenk Str. 37, 38108, Braunschweig, Germany.

I. Introduction

THE study presented in this paper is part of the Collaborative Research Center CRC 880¹, funded by the German Research Foundation DFG. It is concerned with multi-disciplinary research activities on technologies and configurations for novel low noise commuter aircraft with short take-off and landing (STOL) capabilities. The overall ambition of the CRC 880 is to react on the growing demand for air transportation by aircraft concepts that allow to incorporate up to now not utilized smaller airports in populated areas. Short range aircrafts are considered with the objective to make them competitive to ground transportation while meeting all environmental standards with the potential to reduce door-to-door travel time. The specific challenge is to derive aircraft configurations with extraordinary airfield performance and low noise emissions that are as fuel efficient as feasible². The research activities are carried out in cooperation between the Technical University of Braunschweig, the Leibniz University of Hannover, and the German Aerospace Center (DLR). The focus is laid on exploring fundamental aspects of related technologies, configurations, and their smart combination, rather than to design specific aircrafts.

To approach the afore mentioned purposes, two aircraft concepts are investigated in the CRC 880 that aim to comply with the requirements with slightly varying emphasis. They are designated as reference configuration 2 (REF-2) and reference configuration 3 (REF-3), respectively. Figure 1 depicts both aircraft variants as defined throughout preliminary design studies of the CRC 880, see also Ref 3.

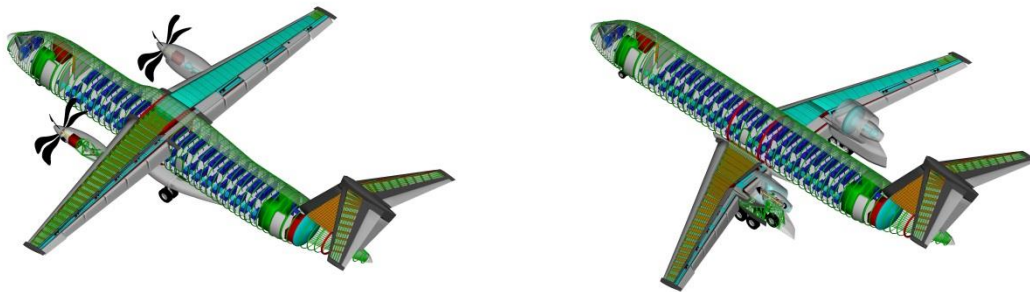


Figure 1: REF-2 (left) and REF-3 (right) aircraft in landing configuration.

The main underlying top level aircraft requirements are a capacity of 100 passengers, a range of about 1100 nautical miles, and an airfield requirement of 800 m. While REF-2 is cruising at a design Mach number of $M = 0.74$, REF-3 has an increased design Mach number of $M = 0.78$. Consequently, REF-3 features a leading edge sweep of 26° , while the high wing of REF-2 is only moderately swept back by 10° . A UHBR-engine with a bypass ratio of 17 is utilized to power REF-3, in contrast, the REF-2 high wing configuration is powered by a turboprop engine. The rationale to define and investigate the REF-3 configuration is driven by two aspects. First, the configuration offers a noise mitigation potential by shielding the fan noise. It also offers the benefits of a ducted propulsor with low jet velocities instead of the open prop engine of REF-2. The second aspect related to REF-3 concerns the aerodynamic potential to efficiently use the interference of a low velocity fan inlet streamtube with the suction side of the wing in cruise conditions to reduce the wave drag as outlined in Ref. 4. Figure 2 shows REF-3 with an engine position that is based on numerical investigations to yield efficient high speed cruising properties, see Ref. 5.

Based on further refinement studies of the REF-3 cruise configuration⁶, the present paper describes preparatory investigations to assess the low speed high lift performance of the swept back low wing configuration REF-3. The high lift system consists of active circulation controlled flaps coupled with a flexible leading edge device (droop nose). The well known concept of circulation control is used to mitigate the separation of the flow at the highly deflected flaps by properly blowing an air jet over a Coanda surface. The Coanda effect allows the jet to follow the contour, bending the trailing edge flow downwards and thus increase lift generation. An overview of aircraft applications of circulation control systems and related numerical and experimental investigations is provided in Ref. 7. The detailed aerodynamic design work of the baseline high lift system with a single hinged flap for the reference wing is described in Ref. 8 and 9. The droop nose is essential to support the high circulation provided by the Coanda flap, allow higher attitudes at take-off and landing conditions, and prevent premature stall. The high lift system has been integrated at the REF-2 configuration and delivered high lift properties that fulfilled the above mentioned requirements¹⁰. The steps to adapt the high lift system to the REF-3 configuration are described as well as numerical studies focusing on a reduced chord hinged flap system with circulation control.



Figure 2: CRC 880 REF-3 configuration

II. Reference Configuration and Low Speed Geometry Design

The high speed layout of the reference configuration REF-3 is the starting point for the present study. It has been designed according to the CRC 880 Technical Data Sheet³ by using CATIA V5. The overall set-up features a 100-passenger aircraft for short haul flights, with a low wing arrangement and two UHBR turbofan engines mounted over the wing, aft of the trailing edge at 31% half span. The engine contours and thermodynamic properties have been elaborated by the Institute of Jet Propulsion and Turbomachinery (IFAS) of the Technical University of Braunschweig. They BPR of the engines is 17, they provide a maximum thrust of 2 x 134 kN at take-off conditions in order to support the STOL characteristics of the aircraft. The main aircraft dimensions are listed in Table 1.

Table 1: Main dimensions of the CRC 880 REF-3 configuration

half span, s	[m]	14.37
wing reference area, A	[m ²]	99
reference chord, c_{ref}	[m]	3,8
aspect ratio, Λ	[-]	8.4
taper ratio, λ	[-]	0.321
Leading edge sweep, ϕ_{LE}	[°]	26
fuselage length, l_{Fu}	[m]	33.2
flap deflection angle, δ_s	[°]	60.0
aileron deflection angle, δ_{ai}	[°]	45.0
Nacelle diameter (max)	[m]	2,02

Another distinctive feature of REF-3 configuration is the pylon layout, since the main landing gears are housed in the lower segment of the pylon extending its size considerably beyond the typical engine mounting device as can be seen in Figure 2. At this point of the investigations the airfield requirements for the Ref-3 configuration have been relaxed to 950 m due to an expected performance degradation compared to REF-2 because of the higher wing sweep and the lack of the propeller slipstream effect. As a first step of the high lift study, the flap system has been implemented in the REF-3 wing geometry. For this purpose, the REF-2 high lift system was used as reference model. Its Coanda flaps were implemented on the REF-3 moderately swept trailing edges but adapted to the local chord lengths. The baseline section of high-lift landing configuration is sketched in Figure 3. The Coanda effect is amplified by the stream of accelerated flow exiting tangentially over the convex upper surface of the flap.

A design and optimization study for the wing/flap section geometry resulted in a flap length of 25% chord length¹¹. The corresponding slot height for the jet blowing is $h/c=0.0006$, where h is the slot height and c is the chord length. For the present first adaptation of the circulation control high lift arrangement to the REF-3 configuration, a reduced local flap chord of 13% local chord has been considered with a slot height of $h/c=0.0011$.

The rationale is to assess the high lift performance for a reduced flap chord in order to provide more freedom for the design of the fixed wing component which is strongly influenced by the pylon and engine flow.

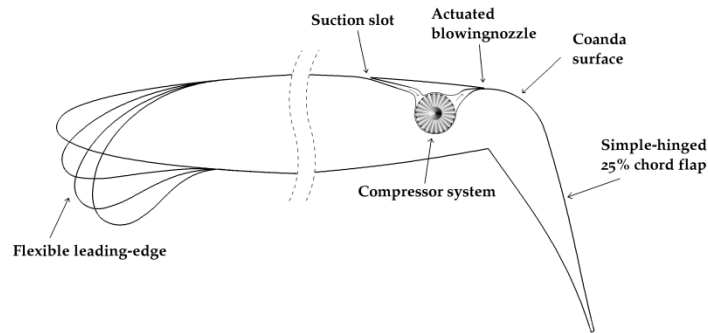


Figure 3. Sketch of the baseline high lift section with droop nose and Coanda flap.

The characteristics of the outer flow which mixes with the Coanda jet are essential for the efficiency of the high lift system and for the stall behavior. For low speed high lift conditions, the stall characteristics of the present wing section are determined by the flow at the leading edge of the wing. The high circulation generated by the Coanda control can significantly reduce the stall angle of attack as described by Burnazzi⁹, therefore a leading edge device is essential to ensure a satisfying high lift performance of the configuration in low speed. The droop nose is a flexible morphing leading edge device without gap, in contrast to a conventional slat configuration. It offers acoustic benefits, since the slat gap is a considerable source of noise¹³. The droop nose implementation on REF-2 has been adopted for the REF-3 configuration.

The 3D layout of the high lift system is composed out of six segments, operating from individual plenum chambers that allow an independent adjustment of the wall jets to the local flow conditions, as used for the REF-2 configuration¹². Segment 1 is located inboard of the engine, segments 2 to 5 at the outer wing, as shown in Figure 4.

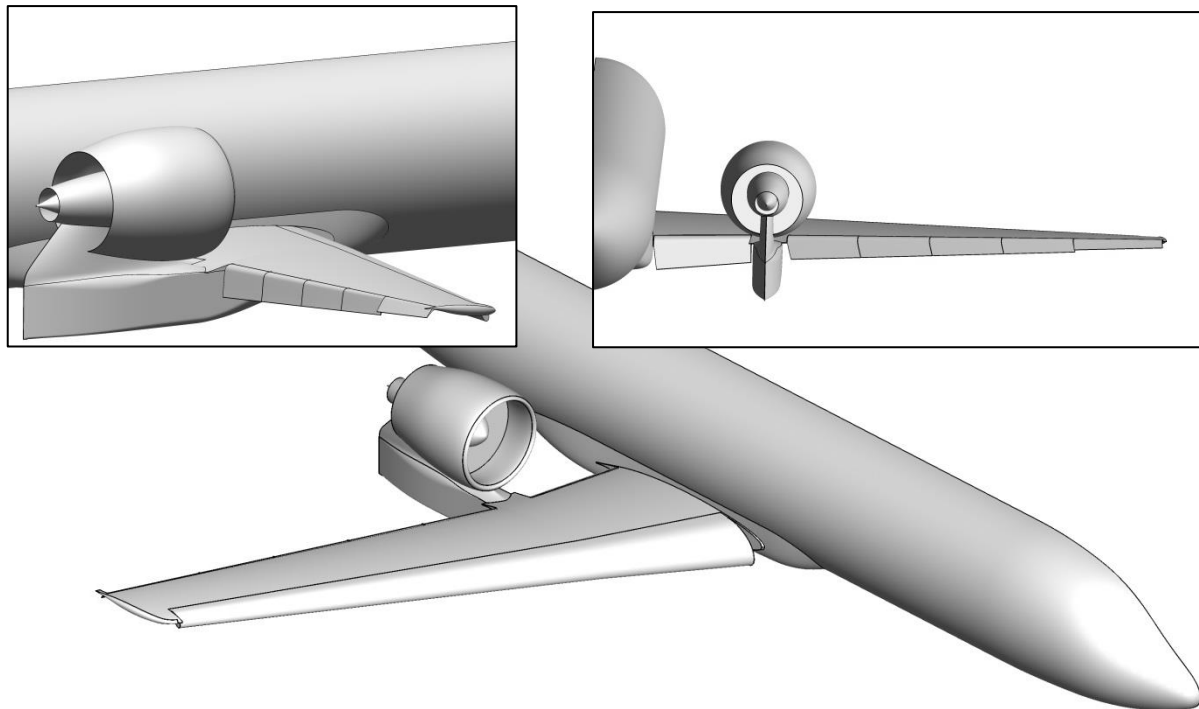


Figure 4. 3D layout of the high lift system with circulation controlled flaps

The flaps in segments 1 - 5 are deflected for 60°. Segment 6 is linked to the aileron. The corresponding deflection of segment 6 in landing configuration is 45°. The droop nose deflection is $\delta_{dn} = 41.8^\circ$.

III. Numerical Method

The numerical simulations are carried out using DLR's flow solver TAU^{14, 15} on hybrid unstructured grids generated with the commercial software CENTAUR¹⁶. Both, the grid generation strategy, and the flow solver adjustments are briefly described in this section.

A. Computational Grids

The computational grids have been generated using the commercial software CENTAUR¹⁶. A hybrid type of grid has been chosen, due to the higher flexibility of hybrid grids in discretizing complex 3D geometries and critical flow features. The grid consists mainly of prisms and tetrahedrons, with structured hexahedra used only to discretize the trailing edges of wing and nacelle and the smallest geometrical features. The local refinement of the surface mesh was done through geometric sources and by using high values of proximity and CAD clustering. This special feature allows the mesh generator to allocate more points in the regions with a more dense presence of different geometrical parts and in correspondence of very small geometrical features. This is essential to ensure that the flow control slots are properly discretized. Figure 5 shows the surface grid on the REF-3 configuration. The aerodynamic surfaces are covered with 3.79 million surface elements.

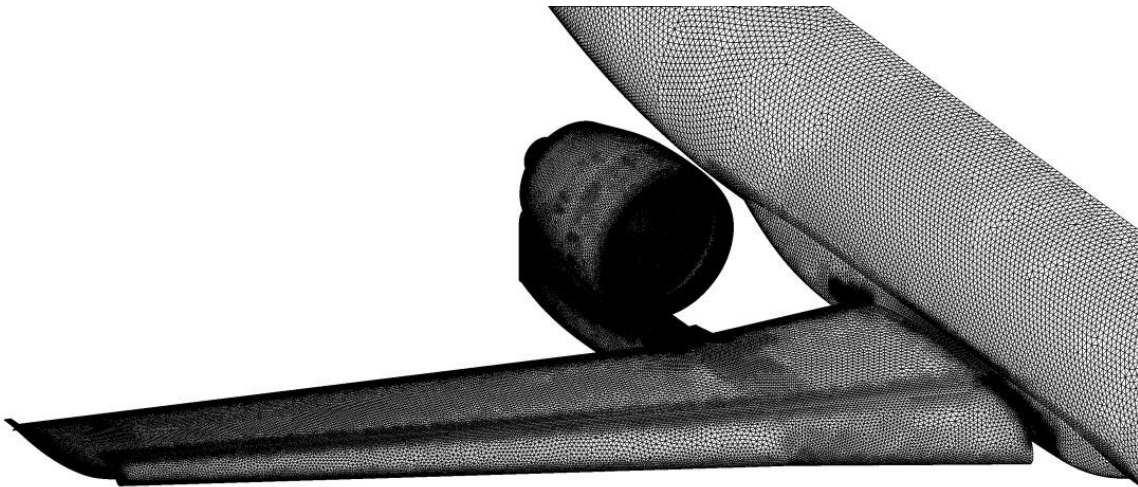


Figure 5. Surface grid for the REF-3 high lift configuration

The generation of the prismatic mesh is the most time consuming part, due to the presence of a large disparity of geometric scales that need to be resolved. In fact, the number of prismatic layers inevitably tends to decrease (chopping phenomenon) from the wing and the flaps to the plenum, due to the very small plenum slot size compared to the overall dimensions of the aircraft components.

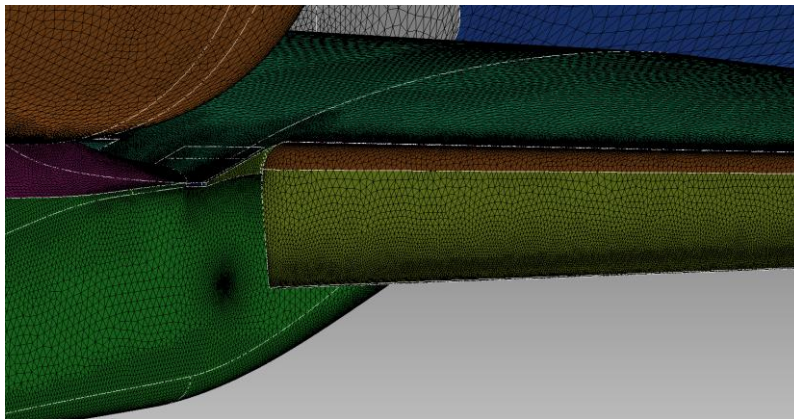


Figure 6. Close-up of the surface grid on the circulation controlled flap, outboards of the engine

A good quality of the prismatic mesh is achieved when the chopping of the prisms in the plenum happens with proper cell angles and the transition from the number of prism layers in the plenum to the one on the flap is as smooth and rapid as possible. A high number of prisms layers, a small initial layer thickness and a small stretching factor of the prisms are used to guarantee a sufficient quality of the mesh. The flap/wing/pylon intersection area outboards of the engine is shown in Figure 6.

Special attention has been dedicated also to the discretization of the engine inflow and outflow planes and to the plenum. High resolution and uniformity of the mesh in these regions are crucial to properly resolve the engine flow and correctly apply the flow solver's inlet/outlet boundary conditions. The surface grid on the outer nacelle, the inlet, the engine core body and plug, as well as on the pylon is depicted in Figure 7.

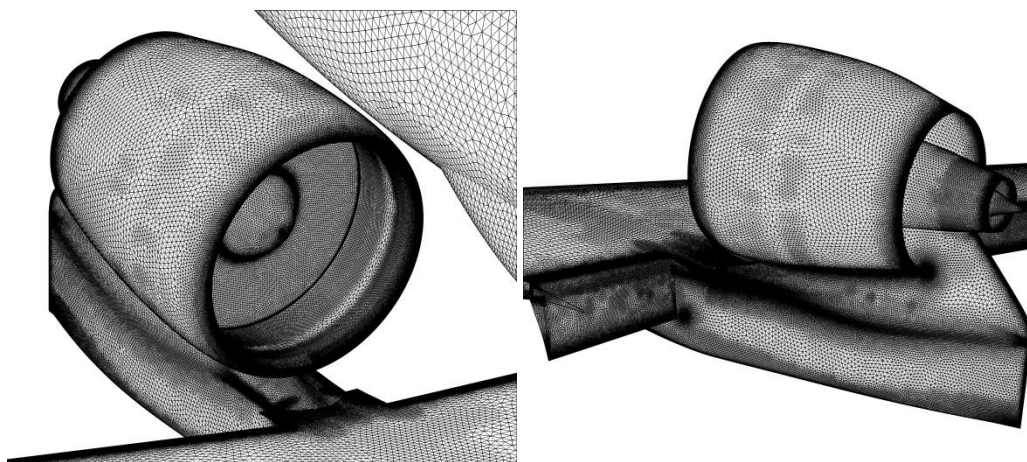


Figure 7. Surface grid for the REF-3 high lift configuration

The overall grid of the full configuration has 68.6 million points. The number of elements is 177.1 million. 113.7 million of these are prims, and 63.8 million tetrahedrons. A y^+ -value of 1 is approached wherever feasible.

B. Flow Solver and Simulations Procedure

The DLR flow solver TAU version 2016.2 is used to solve the steady 3D RANS equations with a finite volume method. Spatial discretization is accomplished with a Jameson second order central scheme, with scalar dissipation in order to ensure more robust simulation and to facilitate its convergence. Time discretization is achieved by the Backward-Euler implicit LUSGS scheme. For turbulence modeling, the Spalart-Allmaras one-equation model in its original formulation¹⁷, but with vortical and rotational flow correction based on the Spalart-Shur¹⁸ is used to preserve comparability with the simulations carried on REF-2 configuration, see Ref. 12. Furthermore, it appears to be a quite suitable model for a preliminary analysis of the considered complex configuration.

The engine settings and operational conditions for the realistic flight test case were calculated by using the GasTurb software¹⁹ and the outputs in terms of massflow and temperature ratio for the fan inlet, and jet pressure and total temperature ratio for the simulation of the fan and core jets. The jet values are prescribed at outlet boundary conditions inside the fan and core duct. The flow simulations are carried out imposing a fixed massflow boundary condition¹⁴.

In order to simulate the circulation control system, the plenum of each segment has been simulated together with a proper duct and slot contour. Within the flow computations, the wall jet exit is initiated by an engine exhaust inside the plenum and the pressure ratio for each slot is given as a boundary condition in order to meet the prescribed mass flow. Each plenum chamber can be operated individually.

For the low speed computations described here, an initial small angle of attack is chosen, where the flow is supposed to have minimal or no separation as a starting alpha for the simulations. Then, an alpha-sweep is conducted with the angle of attack being increased until the maximum angle of attack is reached. Computations are carried out beyond the angle of attack for maximum C_L as far as feasible.

IV. Computational Results

The configurational basis for the present study is a high speed analysis of REF-3 configuration which has resulted in a cruise efficient engine position. The evaluation at low speed performance is in fact essential in order to

verify the feasibility of REF-3 in low speed condition and to assess the compliance with the STOL and noise requirements. The present study is intended to be a first step in this direction and focuses on the landing configuration and conditions, exclusively. The baseline flow conditions and massflow specifications have been derived by the preliminary design activities in the CRC 880. Yet, as mentioned in the introduction, for the present preparatory study, an attempt has been made to evaluate the potential for a reduction of the flap chord compared to the baseline specification. After some details about the flow conditions, the numerical results are discussed in detail.

A. Flow Conditions

In order to assess the high lift performance at landing, a design point with flaps and droop nose fully deflected is selected, and the undercarriage is deployed. For the altitude, a 15 m obstacle height is considered. For simplicity, the undercarriage is neglected in the present investigations. The design speed is 57.1 m/sec at a constant glide slope of 3°. The design data related to the landing test case are summarized in Table 2:

Table 2.: Flow conditions for landing scenario.

M_∞	0.168
Altitude	15 m
Re_c	14,891,614
α - range	-1.88° 20°

The required thrust for each engine is 20.93 KN and the related power setting is 20%. The engines are considered both operative for the present studies. The mass flow rates of the circulation control system at the six flap segments range from 3.09 kg/sec for segment 1 to 0.704 kg/sec at the aileron segment 6. The mass flow rate is increased by about 50% in an attempt to compensate the reduced flap chord length.

The preliminary design studies resulted in a $C_{L,max}$ of 3.24 for the 25% local chord flap, which is not achievable with the present reduced flap chord. It may be worth mentioning that the maximum lift coefficient of the REF-2 high lift configuration has been close to 4.5. Yet, in addition to the larger flap chord, the maximum lift capability of the REF-2 configuration is significantly enhanced by the propeller slipstream and also by the high wing arrangement.

B. Lift Characteristics

In order to get a first impression of the lift characteristic of the REF-3 configuration with the reduced chord flap system, the lift curve is plotted in Figure 8. Lift generation starts already at comparatively small angles of attack due to the impact of the circulation controlled flap system, α_0 is -14°. The linear lift regime extends up to about 7°. Beyond this angle of attack, a smooth lift breakdown is observed with an α_{max} of 15°. A maximum lift coefficient of $C_{L,max} = 2.75$ is reached. The targeted $C_{L,max}$ is also indicated in Figure 8. Obviously, the present reduced chord flap configuration misses the $C_{L,max}$ -target significantly by 49 lcts.

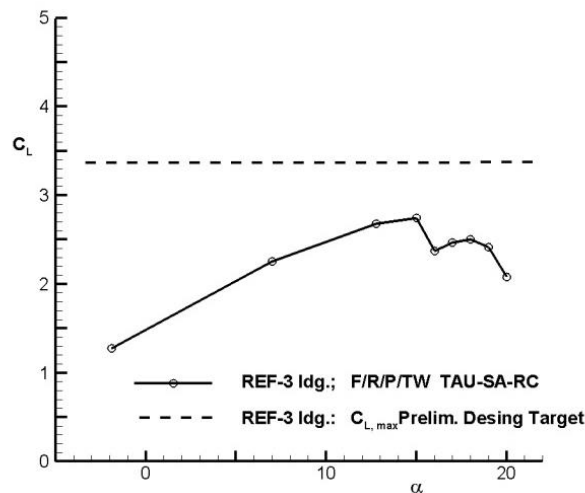


Figure 8. Lift curve for the REF-3 configuration with reduced chord flap

Beyond the initial lift breakdown, lift generation is slightly recovering between $\alpha = 16^\circ$ to 18° with a final clear lift breakdown towards $\alpha \geq 20^\circ$. Surface isobars and streamtraces for $\alpha = 7^\circ, 15^\circ, 16^\circ,$ and 20° are shown in Figure 9 in a front view.

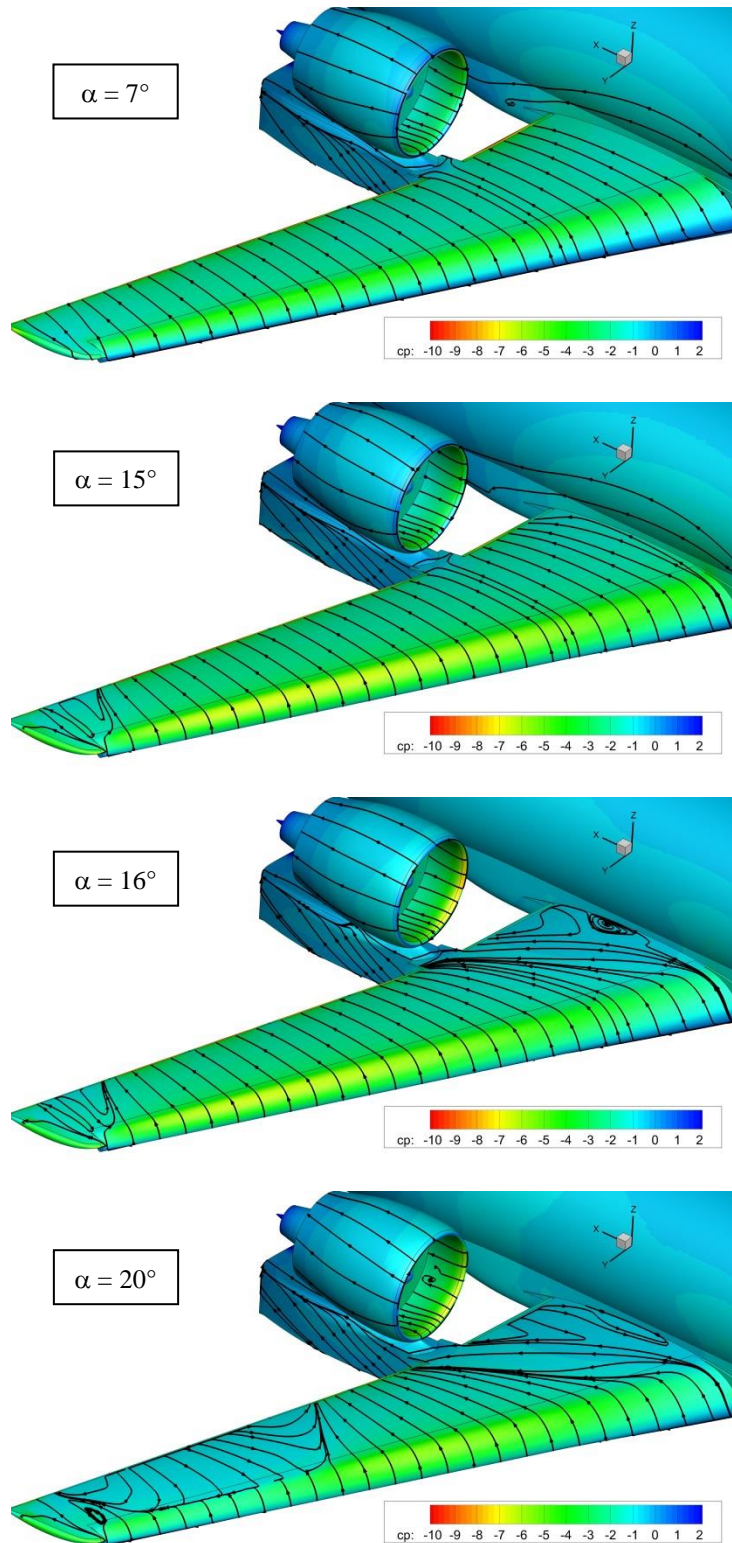


Figure 9. Isobars on the surface and streamlines in a front view for different angles of attack

The angles of attack correspond to conditions in the linear lift range ($\alpha = 7^\circ$), at $C_{L,max}$ ($\alpha = 15^\circ$), and at each of the two lift breakdowns ($\alpha = 16^\circ, 20^\circ$), observed in Figure 8. As expected the flow is smooth and attached at $\alpha = 7^\circ$.

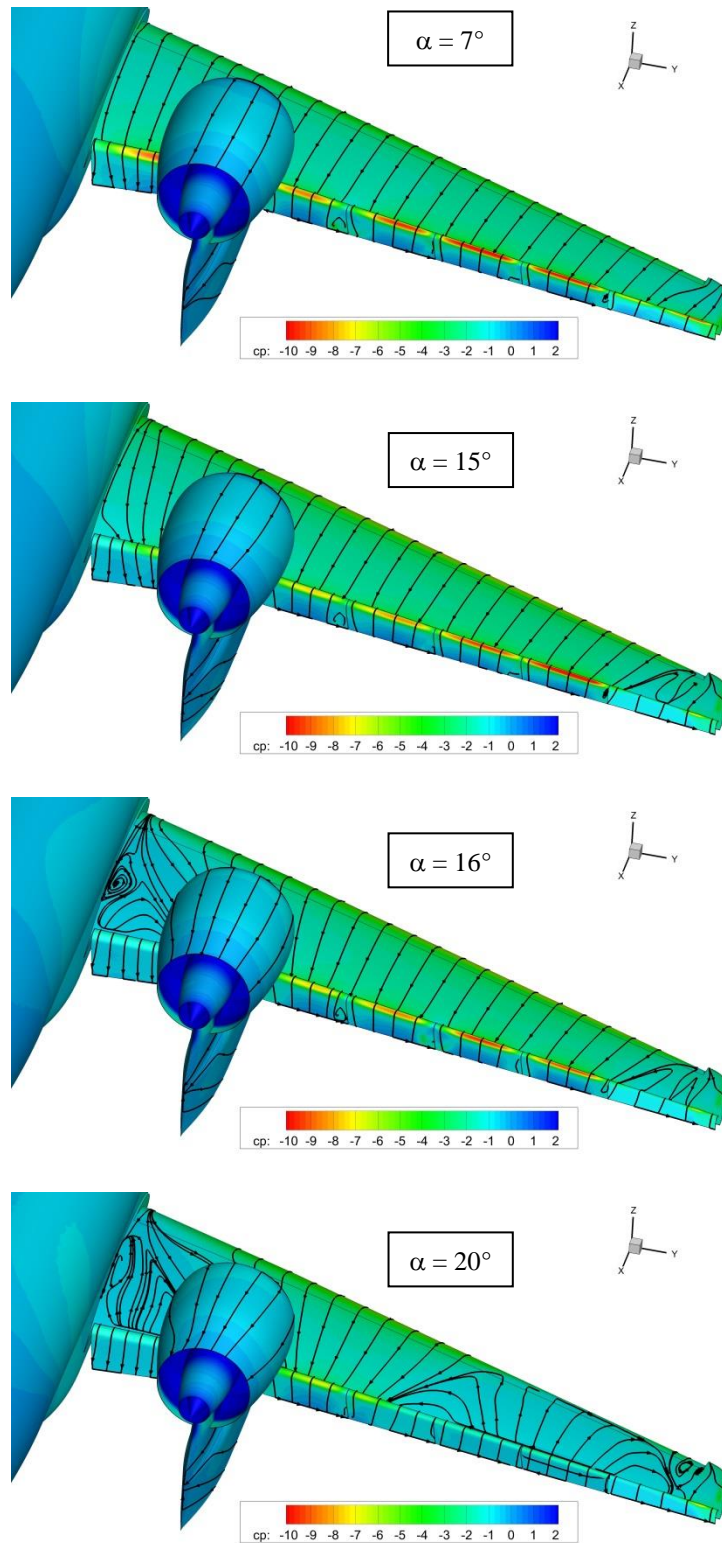


Figure 10. Isobars on the surface and streamlines in a rear view for different angles of attack

A low pressure area is visible at the droop nose knuckle, extending over the whole span. For $\alpha = 15^\circ$, the suction peaks at the droop nose become stronger in the mid to outer part of the wing, while the flow is still attached. A tendency for flow separation is observed at the wing tip. As the stream patterns for $\alpha = 16^\circ$ prove, the first moderate lift breakdown is caused by a strong separation at the inboard wing, starting at about 40% root chord. The area of separated flow widens considerable towards the trailing edge and displaces the attached flow towards the engine. The final lift breakdown at $\alpha = 20^\circ$ is caused by a strong and extended area of separated flow at the outboard wing. This separation starts already at the rear part of the droop nose and extend laterally towards the wing tip.

The flow on the pylon remains attached for all evaluated angles of attack. For both angles of attack beyond α_{\max} , a suction area is developing at the inner part of the nacelle in the lower sector. As symmetric flow conditions are considered and the engines don't have any toe-angles, it is probably related to the inboard separation and its extent above the wing surface.

Figure 10 provides a view from the rear of the same isobar distribution for the considered four angles of attack. This view allows an assessment of the circulation controlled plain flap. The high jet velocity through the slots for segments 1 to 5 is clearly visible by the red color, indicating a low pressure high velocity area. Only a weak acceleration is observed for the aileron segment 6. The gaps between the flap segments cause the suction areas to collapse locally. As a consequence, a trend for separation at the gaps of the flap segments is visible in Figure 10.

Obviously, the general trends of the development of the flowfield with increasing angle of attack are present as discussed before. The red high velocity, low pressure areas at the slots of the circulation control system are most pronounced at segments 3 to 5. Towards the inboard segments 1 and 2, the suction level is considerably reduced with increasing angle of attack. This might serve as an indication that there is a need for a re-adjustment of the plenum pressures and massflows for the two inboard flap segments. Apart from the segment gaps, the flow along all flap segments remains attached until the highest angles of attack. This includes the aileron segment 6, which is essential to ensure control authority of the aileron at stall. The strong and extended separation is limited to the fixed wing itself.

For the engine nacelle, the flow is attached at the outboard surface until the highest angle of attack. Yet, as a view from the symmetry plane in Figure 11 reveals, a considerable area of separated flow is present at the nacelle for $\alpha = 20^\circ$. It is located in the lower aft part at the inboard surface of the nacelle. Obviously, there is some aerodynamic interference between the large triangular area of separated flow at the inboard wing and the engine nacelle, which needs further investigations. Nevertheless, it has to be kept in mind that this separation occurs at angles of attack far beyond maximum lift conditions.

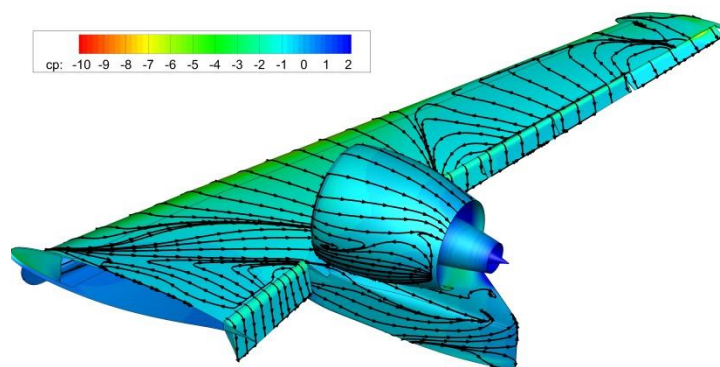


Figure 11. Isobars on the surface and streamlines in a rear view from the symmetry plane for $\alpha = 20^\circ$

C. Wing Pressure Distributions

In order to discuss the section wise lift generation and aerodynamic interference effects due to the presence of the engine, three pressure sections are analyzed for the angles of attack considered before except for $\alpha = 20^\circ$. The sections are located at $\eta = 0.27$, 0.33 , and 0.66 , see also Figure 12. The engine is mounted at 31% half span. Note that the section at $\eta = 0.33$ doesn't have a flap element. The sections at $\eta = 0.27$ and 0.33 may serve to discuss

engine/airframe interference effects, while the section at $\eta = 0.66$ is representative for a widely undisturbed swept wing segment.

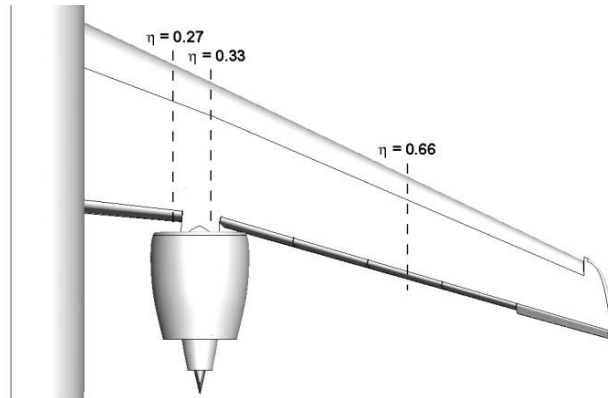


Figure 12. Location of pressure sections for REF-3 configuration

The pressure distributions for these three sections are depicted in Figure 13. The inboard section at $\eta = 0.66$ has a plain flap and a droop nose element.

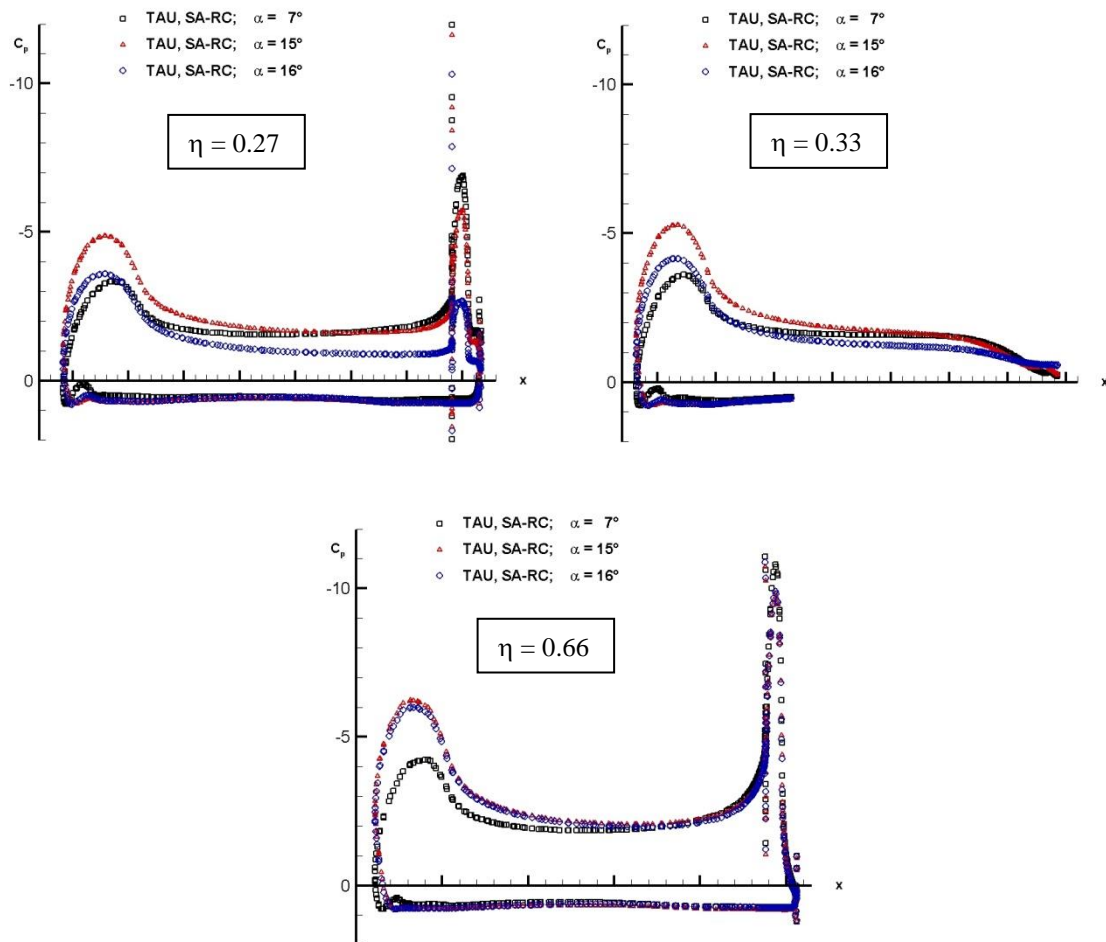


Figure 13. Pressure distributions in 3 cuts of the wing at different angles of attack

As already discussed in the three-dimensional analysis in Figure 9, the buildup of the rounded suction peak in the nose region of this section is rather moderate. The highest suction level is observed at α_{\max} . The effect of the circulation control system is clearly visible at the plain flap. The high velocity wall jet causes a suction peak that is significantly higher than the one at the nose. In this case, the highest suction level is reached for the smallest evaluated angle of attack $\alpha = 7^\circ$. Again, this is consistent with the observation in Figure 10. Beyond maximum lift, both suction peaks at the nose and the flap collapse. Also the pressure level at the wing upper surface is higher due to the root separation inboard of the section and the induced strong crossflow, see Figure 9. There is also an indication for a limited separation at the trailing edge of the flap for $\alpha = 16^\circ$.

The trends at the leading edge region of the section outboard of the engine at $\eta = 0.33$ are quite similar. The differences in the pressure distributions in the aft part of the section are considerably smaller than inboard of the engine. No separation is visible for $\alpha = 7^\circ$ and 15° , while the flow seems to be close to reversal for $\alpha = 16^\circ$.

The development of the pressure distribution at the outboard section at $\eta = 0.66$ with respect to angle of attack is unaffected of the presence of the engine or end effects of the wing. With the presence of the circulation control flap, the typical pressure distribution is observed, featuring a low pressure area in the front part of the section and distinct suction peaks at the plain flap, which are considerably higher those in the front part. The lift breakdown, in this case, the difference between the red and the blue symbols corresponding to $\alpha = 15^\circ$ and 16° , respectively, is very weak. Again, this finding is consistent with the isobar plots in Figure 9. The lift breakdown at the mid wing is occurring at higher angles of attack as can be seen in Figure 9 for $\alpha = 20^\circ$.

V. Conclusion

A preliminary low speed high lift investigation of a low noise short range aircraft with STOL properties has been carried out. The configuration is characterized by two UHBR-engines mounted at 31% half span above the low wing's trailing edge. Lift generation for low speed high lift conditions is enhanced by a circulation controlled plain flap trailing edge system and a droop nose at the leading edge. The circulation controlled plain flap is subdivided in 6 segments. For the considered landing conditions, all segments have a deflection angle of 60° , with the most outboard segment that serves as a flaperon deflected by only 45° . In order to assess the potential of a reduced chord trailing edge device, a plain flap with 13% instead of the 25% local chord length as a reference preliminary design value has been investigated.

The lift characteristics is as expected for a high lift system with circulation control, revealing a strongly negative α_0 . Lift breakdown occurs first at the fixed wing inboards of the engine. Maximum lift coefficient is reached in a rather smooth way. Final lift breakdown occurs at about 3° larger angles of attack. It is triggered by an extended separation at the mid to outer part of the fixed wing. The reduced chord flaps remain widely attached until the highest evaluated angles of attack. Although the outer wing also features a separated region, this stall characteristics holds promise to maintain controllability at the aileron beyond α_{\max} .

Yet, the computed maximum lift capabilities fall short of the requirements by about 20%. The maximum lift coefficient of the reduced chord plain flap with circulation control support is in the range of state-of-the-art conventional mechanical systems with a single slotted Fowler flap and a slat. The results indicate some potential to further increase the high lift capabilities by an improved spanwise adjustment and an overall increase of the blowing coefficients of the circulation control system. Moreover, a grid refinement study has to be carried out to ensure that the local grid resolution at the flap and droop nose is sufficient to capture the suction regions appropriately.

At present a numerical study is conducted for the REF-3 configuration with the baseline 25% chord plain flap trailing edge device. Preliminary results indicate that this high lift system is able to meet the maximum lift requirements defined by the preliminary aircraft design activities in the CRC 880.

Acknowledgments

Financial support has been provided by the German Research Foundation (Deutsche Forschungsgemeinschaft – DFG) in the framework of the Sonderforschungsbereich 880. In the adjusting the computations, Dr. Stefan Melber-Wilkending and Dennis Keller from the Transport Aircrafts department of DLR Braunschweig gave very valuable support.

References.

- ¹F. Kauth, J. R. Seume, R. Radespiel, „Progress in Efficient Active High-Lift“, *35th AIAA Applied Aerodynamics Conference*, Denver, Colorado, 5-9 June 2017, AIAA 2017-3559, 2017.
- ²R. Radespiel, W. Heinze, L. Bertsch, „High-Lift Research for Future Transport Aircraft“, 66. Deutschen Luft-und Raumfahrtkongress, 5th – 7th September, Munich, 2017
- ³W. Heinze, T. Weiss, “Main Data Sheet. A/C Type: SFB 880 Reference Aircraft REF3-2015”, 2015.
- ⁴J. Hooker, A. Wick, C. Zeune, A. Agelastos, “Over-the-Wing Nacelles Installations for Improved Energy Efficiency”, 31st AIAA Applied Aerodynamics Conference, San Diego, CA, 2013.
- ⁵L. Savoni, R. Rudnik, Aerodynamic Assessment of Pylon-Mounted Over-the-Wing Nacelle Installations on a STOL Commercial Aircraft Concept, in A. Dillmann et al. (eds.), *New Results in Numerical and Experimental Fluid Mechanics XI, Notes on Numerical Fluid Mechanics and Multidisciplinary Design 136*, DOI 10.1007/978-3-319-64519-3_5, 2018
- ⁶L. Savoni, R. Rudnik, „Pylon Design for a Short Range Transport Aircraft with Over-the-Wing Mounted UHBR Engines”, AIAA SciTech Forum, 8–12 January 2018, Kissimmee, Florida, AIAA 2018-3559, 2018
- ⁷G. S. Jones, R. D. Joslin, “Proceedings of the 2004 NASA/ONR Circulation Control Workshop”, Proceedings of a workshop sponsored by the National Aeronautics and Space Administration and Office of Naval Research, Arlington, Virginia held at Radisson-Hampton, Hampton, Virginia, March 16 – 17, 2004, NASA/CP-2005-213509/PT1, 2005
- ⁸K.C. Pfingsten, R.D. Cecora, R. Radespiel, „An Experimental Investigation of a Gapless High-Lift System Using Circulation Control“, CEAS/CATnet II Conference, Bremen, Germany, 2009, pp. 2, 41, 42, 44.
- ⁹M. Burnazzi, “Design of Efficient High-Lift Configurations with Coanda Flaps”, Niedersächsisches Forschungszentrum für Luftfahrt, Forschungsbericht 2016-11.
- ¹⁰D. Keller, R. Rudnik, “Numerical investigations of aerodynamic properties of a propeller blown circulation control system on a high wing aircraft”, 50th 3AF International Conference on Applied Aerodynamics, Toulouse, 23rd -30th March – 1st April 2015.
- ¹¹C. Jensch, K.C. Pfingsten, R. Radespiel, „Numerical investigation of leading edge blowing and optimization of the slot and flap geometry for a circulation control airfoil“, in „New Results in Experimental and Numerical Fluid Mechanics VII, Vol. 112, SPRINGER, 2010, pp. 183-190.
- ¹²D. Keller, R. Rudnik, “Numerical Investigation of Engine Effects on a Transport Aircraft with Circulation Control”, *Journal of Aircraft*, Vol. 52, No. 2, March-April 2015.
- ¹³M. Pott-Pollenske et al., „Slat Noise Reduction by means of Adaptive Leading Edge Devices”, in “Aircraft Noise Reduction by Flow Control and Active/Adaptive Techniques”, Vilnius, Litauen, 2014, pp. 15-49.
- ¹⁴TAU-Code Users Guide, Release 2015.1.0, 2015.
- ¹⁵J. Blazek, “Computational Fluid Dynamics: Principles and Applications”, ELSEVIER, 2001.
- ¹⁶CentaurSoft Homepage, www.centaursoft.com.
- ¹⁷Spalart, P. and Allmaras, S., “A One–Equation Turbulence Model for Aerodynamic–Flows,” AIAA Paper 92–0439, 1992.
- ¹⁸Spalart, P. and Shur, M., “On the sensitization of turbulence models to rotation and curvature,” Vol. 1 of *Aerospace Science and Technology*, 1997, pp. 297–302.
- ¹⁹GasTurb Version 12, www.gasturb.de